# Finite-temperature fidelity and von Neumann entropy in the honeycomb spin lattice with quantum Ising interaction

Yan-Wei Dai,[1,2] Qian-Qian Shi,[2,1] Sam Young Cho,[2,3,*] Murray T. Batchelor,[2,4] and Huan-Qiang Zhou[2,3]

[1]*College of Materials Science and Engineering, Chongqing University, Chongqing 400044, China*

[2]*Centre for Modern Physics, Chongqing University, Chongqing 400044, China*

[3]*Department of Physics, Chongqing University, Chongqing 400044, China*

[4]*Mathematical Sciences Institute and Department of Theoretical Physics, Research School of Physics and Engineering, The Australian National University, Canberra ACT 2601, Australia*

(Received 26 January 2017; revised manuscript received 27 April 2017; published 14 June 2017)

The finite-temperature phase diagram is obtained for an infinite honeycomb lattice with spin-1/2 Ising interaction $J$ by using thermal-state fidelity and the von Neumann entropy based on the infinite projected entangled pair state algorithm with ancillas. The tensor network representation of the fidelity, which is defined as an overlap measurement between two thermal states, is presented for thermal states on the honeycomb lattice. We show that the fidelity per lattice site and the von Neumann entropy can capture the phase transition temperatures for an applied magnetic field, consistent with the transition temperatures obtained via the transverse magnetizations, which indicates that a continuous phase transition occurs in the system. In the temperature-magnetic field plane, the phase boundary for finite temperature is found to be well approximated by the functional form $(k_B T_c)^2 + h_c^2/2 = aJ^2$ with a single numerical fitting coefficient $a = 2.298(7)$, where $T_c$ and $h_c$ are the critical temperature and field with Boltzmann constant $k_B$. The critical temperature in the absence of magnetic field is estimated as $k_B T_c/J = \sqrt{a} \simeq 1.516(2)$, compared with the exact result $k_B T_c/J = 1.51865\ldots$. For the quantum state at zero temperature, this phase boundary function gives the critical field estimate $h_c/J = \sqrt{2a} \simeq 2.144(3)$, compared to the known value $h_c/J = 2.13250(4)$ calculated from a cluster Monte Carlo approach.

DOI: 10.1103/PhysRevB.95.214409

## I. INTRODUCTION

Since Landau's spontaneous symmetry breaking theory was developed, the Landau-Ginzburg-Wilson theory [1] has been pivotal to understanding phase transitions in quantum many-body systems [2,3]. In the last decade, quantum phase transitions have been intensively and extensively investigated to provide a deeper understanding of quantum critical phenomena from the perspective of quantum information [4]. Significant progress in understanding measures of quantum entanglement, i.e., purely quantum correlations absent in classical systems, has been achieved in connection with quantum phase transitions. Especially, for any finite-size one-dimensional spin system, it was shown that the von Neumann entropy quantifies the bipartite entanglement between the two partitions of the system, with logarithmic scaling behavior with respect to the partitioned system size, and a scaling prefactor proportional to the central charge $c$, a fundamental quantity in conformal field theory and critical phenomena [5–9]. Recently, geometric measures quantifying multipartite entanglement have been shown to scale inversely with the system size [10–13] where the scaling factor is universally connected to the minimum Affleck-Ludwig boundary entropy [14], i.e., the minimum ground-state degeneracy corresponding to one of the boundary conformal field theories compatible with the bulk criticality [15]. Quantum entanglement has then been used as a marker and characteristic property of quantum phase transitions driven by quantum fluctuations in one-dimensional quantum many-body systems.

As another way to characterize quantum phase transitions, quantum fidelity, defined as an overlap measurement between quantum states, has been introduced from the basic notion of quantum mechanics based on quantum measurement in quantum information [16–26]. In order to explore quantum phase transitions from the viewpoint of quantum fidelity, various quantum fidelity approaches have been suggested, such as fidelity per lattice site (FLS) [18], reduced fidelity [20], fidelity susceptibility [21], density-functional fidelity [22], and operator fidelity [23]. Quantum fidelity approaches have been shown to capture critical behavior in a range of systems and provide an alternative marker of quantum phase transitions without knowing any detailed broken symmetry. Especially, the ground-state FLS has been demonstrated to capture drastic changes of the ground-state wave functions in the vicinity of a critical point, even for those which cannot be described in the framework of Landau-Ginzburg-Wilson theory, such as a Beresinskii-Kosterlitz-Thouless transitions [27] and topological quantum phase transitions [28] in quantum one-dimensional many-body systems. Further, quantum fidelity has also manifested the relation between degenerate ground states and spontaneous symmetry breaking [29,30].

Such developments in understanding quantum phase transitions could be applied towards understanding finite-temperature phase transitions more deeply from the perspectives of entanglement and fidelity. It is then natural to ask whether such approaches can be generalized to characterize finite-temperature phase transitions. As a measure of similarity between two quantum states, quantum fidelity defined by the overlap function between them can be generalized to a fidelity defined by an overlap function between two

*sycho@cqu.edu.cn

 

thermal density matrices in thermodynamic systems at finite temperature. As is well-known, at zero temperature, ground states in different phases should be orthogonal due to their distinguishability in the thermodynamic limit. This fact allows the quantum fidelity between quantum many-body states in different phases signaling quantum phase transitions from an abrupt change of the fidelity when system parameters vary through a phase transition point. Similar to the quantum fidelity, the thermal fidelity may exhibit a singular behavior for a finite-temperature phase transition. Based on such a thermal fidelity, a fidelity susceptibility has been mainly investigated [31–38] and a thermal fidelity per lattice site has been studied very recently in the Kitaev honeycomb model [39]. A thermal reduced density matrix can be defined from the thermal density matrix. For finite-temperature phase transitions, a von Neumann entropy defined by the thermal reduced density matrix at finite temperature can exhibit a similar behavior to the von Neumann entropy at zero temperature. A few investigations have been carried out to use the von Neumann entropy for finite-temperature phase transitions [40–44].

In this paper, we numerically investigate the finite-temperature phase transition for the honeycomb lattice with spin-1/2 Ising interactions. To describe the honeycomb spin lattice, we employ the infinite projected entangled pair state (iPEPS) representation [45] with ancillas [46,47]. The ancilla states have been introduced to include finite-temperature effects. Thermal states can be expressed in the Hilbert space enlarged due to the ancilla states. In terms of a thermal density matrix given by the thermal states, we introduce a thermal fidelity and von Neumann entropy at finite temperature. We show that the thermal fidelity and von Neumann entropy can detect finite-temperature phase transitions. The detected phase transition points in the temperature-magnetic field plane are discussed by introducing a phase boundary function with a single numerical constant. From this, the estimated quantum critical point at zero temperature and the estimated critical temperature in zero magnetic field are shown to be consistent with the Monte Carlo calculation [48] and the exact result [49,50], respectively.

Our paper is organized as follows. In Sec. II, we introduce the honeycomb lattice with Ising interactions. A brief explanation is given for the extension of the iPEPS to thermal projected entangled pair states (tPEPS) with ancillas [46] in the enlarged Hilbert space at finite temperature on the honeycomb lattice. This approach allows us to define a thermal state of the system including finite-temperature effects. In Sec. III, we outline the numerical procedure for the tensor-network-based thermal-fidelity and discuss the singular behavior of thermal-fidelity indicating the occurrence of a phase transition. The singular behavior of the von Neumann entropy at the phase transition temperature is discussed in Sec. IV. The transition temperatures obtained are shown to be consistent with those calculated from the magnetization in Sec. V. Section VI is devoted to the discussion of the phase boundary and the estimates of the quantum critical field at zero temperature and critical temperature in the absence of the magnetic field. A summary and remarks are given in Sec. VI.

## II. HONEYCOMB LATTICE WITH QUANTUM ISING INTERACTION

We consider an infinite honeycomb lattice with spin-1/2 Ising exchange interaction in the presence of a transverse magnetic field. The Hamiltonian defined on the honeycomb lattice can be written as

$$H = H_{zz} + H_x, \tag{1}$$

where the spin exchange interaction $H_{zz}$ and the interaction with the magnetic field $H_x$ are respectively given by

$$H_{zz} = -J \sum_{\langle s,s' \rangle} \sigma_z^s \sigma_z^{s'}, \tag{2a}$$

$$H_x = -h \sum_s \sigma_x^s \tag{2b}$$

with the strength of the spin exchange interaction $J > 0$ and the transverse magnetic field $h$. Here, $\sigma_z^s$ and $\sigma_x^s$ are the spin-1/2 Pauli matrices at site $s$. $\langle s,s' \rangle$ runs over all nearest-neighbor pairs on the honeycomb lattice. At zero temperature $T = 0$, if the spin exchange interaction $J$ is much bigger than the magnetic field $h$, i.e., $J \gg h$, the Hamiltonian can be reduced to $H \approx -\sum_{\langle s,s' \rangle} \sigma_z^s \sigma_z^{s'}$ on the honeycomb lattice. The Hamiltonian becomes $H \approx -\sum_s \sigma_x^s$ for $J \ll h$. Then the system can undergo a quantum phase transition due to a spontaneous $Z_2$-symmetry breaking, which is characterized by a nonzero transverse magnetization $M_z = \langle \psi | \sigma_z | \psi \rangle$ with a ground-state wave function $|\psi\rangle$ at zero temperature. The quantum critical point was estimated as $h_c/J = 2.13250(4)$ from the cluster Monte Carlo approach [48]. The Ising model on the honeycomb lattice has the exact critical temperature [49,50]

$$k_B T_c / J = \frac{2}{\ln(2+\sqrt{3})} = 1.51865\ldots \tag{3}$$

in the absence of the transverse magnetic field ($h = 0$).

### A. Projected entangled pair states representation at finite temperature

To study thermal fidelity, one needs to first obtain thermal states on the infinite honeycomb lattice with the Hamiltonian $H$, where every lattice site is described by $S$ spin states ($i = 1, \ldots, S$). We then employ iPEPS representation with ancillas. By appending each lattice with an ancilla, i.e., accompanying $a$ ancilla states ($a = 1, \ldots, S$), iPEPS can be extended to thermal projected entangled pair states (tPEPS) including finite-temperature effects. Thus the Hilbert space is enlarged due to the ancilla states. Thermal states $|\Psi(\beta)\rangle$ depending on temperature can be defined in the enlarged Hilbert space, where $\beta$ is the inverse temperature, i.e., $1/\beta = k_B T$ with the temperature $T$ and the Boltzmann constant $k_B$. Thermal states $|\Psi(\beta)\rangle$ with ancilla states can be obtained from imaginary time evolution [51] of a pure state in the enlarged Hilbert space spanned by states $\prod_s |i_s, a_s\rangle$, where the product runs over all lattice sites $s$. Actually, the pure state can be defined as a state at infinite temperature, i.e., $|\Psi(0)\rangle = \prod_s (\sum_{i=1}^{S} \frac{1}{\sqrt{S}} |i_s, i_a\rangle)$ because the density of state becomes $\rho(\beta = 0) = \prod_s (\sum_{i=1}^{S} \frac{1}{S} |i_s\rangle\langle i_s|)$ by defining the density of

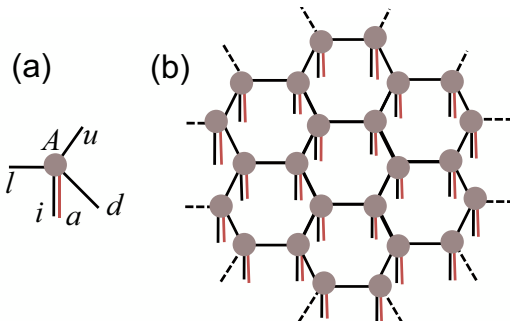


FIG. 1. (a) Pictorial representation of the tensor $A^{ia}_{lur}$. (b) Amplitude $\Psi_{A,B}[\{a_s,i_s\}]$ with all bond indices connecting the nearest-neighbors contracted. The lines connecting two tensors indicate the index contraction.

state at finite temperatures [46] as

$$\rho(\beta) = \mathrm{Tr}_{\mathrm{ancillas}}|\Psi(\beta)\rangle\langle\Psi(\beta)|. \tag{4}$$

Also, the thermal state $|\Psi(\beta)\rangle$ can be written in terms of the pure sate $|\Psi(0)\rangle$ by defining an evolution operator $U(\beta)$, i.e.,

$$|\Psi(\beta)\rangle = U(\beta)|\Psi(0)\rangle. \tag{5}$$

In fact, the density of states at finite temperature can be expressed as $\rho(\beta) \propto e^{-\beta H}$ and then the imaginary time evolution for time $\beta$ with $H/2$ makes it possible to define the imaginary time evolution operator as $U(\beta) = e^{-\beta H/2}$ for the thermal states $|\Psi(\beta)\rangle$.

For our honeycomb lattice, which is two-site translational invariant, a thermal state $|\Psi(\beta)\rangle$ in iPEPS is represented by two tensors $A^{ia}_{lur}(\beta)$ and $B^{ia}_{lrd}(\beta)$, where $S = 2$ and $l,r,u,d = 1,\ldots,D$ are the bond indices with the bond dimension $D$. In the tensor representation, thermal states can then be written as

$$|\Psi(\beta)\rangle = \sum_{a_s,i_s} \Psi_{A,B}[\{a_s,i_s\}] \prod_s |a_s,i_s\rangle, \tag{6}$$

where the sum runs over all indices $i_s,a_s$ at all sites. The tensor contraction of the amplitude $\Psi_{A,B}[\{a_s,i_s\}]$ is shown pictorially on the honeycomb lattice in Fig. 1. For the imaginary time evolution, the initial state $|\Psi(0)\rangle$ defined at infinite temperature ($\beta = 0$) can be chosen as a product state [46]

$$A^{ia}_{lur}(0) = \delta^{ia}\delta_{l0}\delta_{u0}\delta_{r0}, \tag{7a}$$

$$B^{ia}_{lrd}(0) = \delta^{ia}\delta_{l0}\delta_{r0}\delta_{d0} \tag{7b}$$

with the minimal bond dimension $D = 1$. Thus, once one obtains the tensors $A(\beta)$ and $B(\beta)$ for a given temperature after the imaginary time evolution, the thermal states are determined in the tensor representation.

### B. Imaginary time evolution and tensor renormalization

To calculate a thermal state of the system, the idea is to use the imaginary time evolution of the initial state $|\Psi(0)\rangle$ at infinite temperature driven by the Hamiltonian $H$ on the honeycomb lattice. On performing the imaginary time evolution by the time evolution operator $U(\beta) = e^{-\beta H/2}$ on the initial state $|\Psi(0)\rangle$, the second-order Suzuki-Trotter decomposition [52] is employed for an infinitesimal time step as a product

$$U(d\beta) = U_x(d\beta/2)U_{zz}(d\beta)U_x(d\beta/2) + O(d\beta^3), \tag{8}$$

where the evolution gates of the interaction and of the transverse field are defined as $U_x(d\beta) = e^{-H_x d\beta/2}$ and $U_{zz}(d\beta) = e^{-H_{zz}d\beta/2}$, respectively. The single-body evolution gate $U_x(d\beta/2)$ acting on iPEPS with ancillas gives the new tensors $\tilde{A}$ and $\tilde{B}$,

$$\tilde{A}^{ia}_{lur} \propto A^{ia}_{lur} + \epsilon \sum_{j=0,1} \sigma_x^{ij} A^{ja}_{lur}, \tag{9a}$$

$$\tilde{B}^{ia}_{lrd} \propto B^{ia}_{lrd} + \epsilon \sum_{j=0,1} \sigma_x^{ij} B^{ja}_{lrd}, \tag{9b}$$

where $\epsilon = \tanh[hd\beta/4]$ and the dimensions of the new tensors $\tilde{A}^{ia}_{lur}$ and $\tilde{B}^{ia}_{lrd}$ are kept as $D$. While the two-body evolution gate $U_{zz}(d\beta)$ acting on the iPEPS with ancillas gives the new tensors $\tilde{A}$ and $\tilde{B}$ are

$$\tilde{A}^{ia}_{2l+s_l,2u+s_u,2r+s_r} \propto \epsilon^{s/2}(-1)^{is} A^{ia}_{lur}, \tag{10a}$$

$$\tilde{B}^{ia}_{2l+s'_l,2r+s'_r,2d+s'_d} \propto \epsilon^{s'/2}(-1)^{is'} B^{ia}_{lrd}, \tag{10b}$$

where $\epsilon = \tanh[Jd\beta/2]$. The indices satisfy $s = s_l + s_u + s_r$ and $s' = s'_l + s'_r + s'_d$ with $s_l,s_u,s_r,s'_l,s'_r,s'_d \in \{0,1\}$. Equations (10a) and (10b) are an exact map but the tensors $A$ and $B$ are changed from the original $D$ dimension into $2D$ dimension after applying the two-body evolution gate $U_{zz}$, i.e., the new tensors $\tilde{A}$ and $\tilde{B}$ have the bond dimension $2D$ instead of the original bond dimension $D$.

In order to complete updating the tensors for each infinitesimal time step, the new tensors $\tilde{A}$ and $\tilde{B}$ with the bond dimension $2D$ in Eqs. (10a) and (10b) should be reexpressed by another new tensors with the bond dimension $D$. This can be accomplished by using an optimal isometry $W$ that maps from $2D$- back to $D$-dimensions for the new tensors $\tilde{A}$ and $\tilde{B}$ in Eqs. (10a) and (10b) as, respectively,

$$\sum_{l',u',r'=1}^{2D} W_l^{l'} W_u^{u'} W_r^{r'} \tilde{A}^{ia}_{l'u'r'} = A^{ia}_{lur}, \tag{11a}$$

$$\sum_{l',r',d'=1}^{2D} W_l^{l'} W_r^{r'} W_d^{d'} \tilde{B}^{ia}_{l'r'd'} = B^{ia}_{lrd}. \tag{11b}$$

These processes are known as the so-called renormalization of the updating tensors $\tilde{A}$ and $\tilde{B}$. Constructing the optimal isometry $W$ requires calculating the environment tensors of the updating tensor $\tilde{A}$ and $\tilde{B}$. The corner transfer matrix renormalization method [53] is implemented to contract the environmental tensors. The environmental tensors are contracted with each other by indices of dimension $M$ (called environment dimension). Similar implementing processes in Ref. [46] have been then performed to get the updated tensors $A(d\beta)$ and $B(d\beta)$ with truncating back to $D$ from $2D$ dimensions of the updating tensors $\tilde{A}$ and $\tilde{B}$.

## III. THERMAL FIDELITY PER LATTICE SITE

Once the thermal wave functions $|\Psi(\beta)\rangle$ are obtained as a function of temperature from the finite-temperature

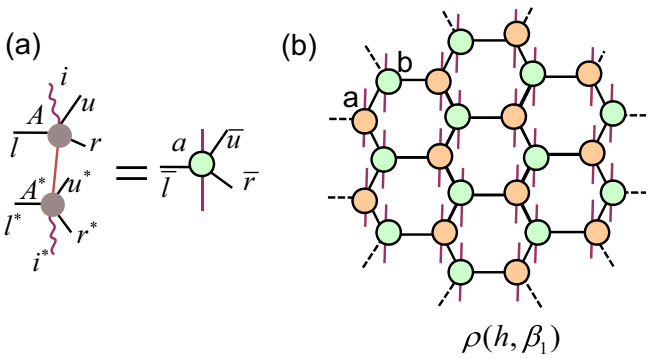


FIG. 2. (a) Contraction of the tensor $A$ and the complex conjugate tensor $A^*$ giving the reduced tensor $a$. (b) Tensor network representation of the density matrix $\rho(h,\beta) = \mathrm{Tr}_{\mathrm{ancillas}}|\Psi(\beta)\rangle\langle\Psi(\beta)|$ by tracing over the ancilla states.

iPEPS algorithm, the thermal density matrix $\rho(\beta) = \mathrm{Tr}_{\mathrm{ancillas}}|\Psi(\beta)\rangle\langle\Psi(\beta)|$ is obtained by taking the trace over the ancillas state of thermal wave functions. The thermal density matrix $\rho(\beta)$ can then be presented by the reduced tensors $a$ (denoted by orange circles) and $b$ (denoted by green circles) in the tensor network representation in Fig. 2(b), where, as is shown in Fig. 2(a), the reduced tensor $a$ is obtained by taking trace over the ancillas index of the tensor $A$ and the complex conjugate tensor $A^*$, and the reduced tensor $b$ (denoted by a green circle) is calculated in the same way. Similar to the quantum fidelity [18,54], the thermal fidelity can be defined in terms of thermal density matrices [32–35,55] as

$$F(\beta_1,\beta_2) = \frac{\mathrm{Tr}\sqrt{\sqrt{\rho(\beta_1)}\,\rho(\beta_2)\,\sqrt{\rho(\beta_1)}}}{\sqrt{\mathrm{Tr}\sqrt{\rho(\beta_1)}\,\mathrm{Tr}\rho(\beta_2)\,\mathrm{Tr}\sqrt{\rho(\beta_1)}}}. \tag{12}$$

This thermal fidelity has basic properties such as $F(\beta,\beta) = 1$ for equal temperatures and $F(\beta_1,\beta_2) = F(\beta_2,\beta_1)$ for exchanging the thermal states. Also, for relatively large lattice sites, the thermal fidelity can be scaled asymptotically as $F \sim d^L$, where $d$ is a scaling parameter and $L$ is the number of sites. Actually, the scaling parameter $d$ is the averaged thermal-state fidelity per lattice site (tFLS), which is well defined in the thermodynamic limit,

$$d(\beta_1,\beta_2) \equiv \lim_{L\to\infty} F(\beta_1,\beta_2)^{1/L}. \tag{13}$$

From the thermal fidelity, the tFLS satisfies (i) $d(\beta,\beta) = 1$ for the normalization, (ii) $d(\beta_1,\beta_2) = d(\beta_2,\beta_1)$ for the exchange symmetry, and (iii) $0 \leqslant d(\beta_1,\beta_2) \leqslant 1$. At zero temperature $T = 0$, the tFLS reduces to the quantum fidelity per lattice sites (FLS) [18,54] for quantum states.

In performing the calculation of the thermal fidelity, for the density product, i.e., $\rho(\beta_1)^{1/2}\rho(\beta_2)\rho(\beta_1)^{1/2}$, the two basic cell structures can be constructed on the honeycomb lattice with the transfer matrices $E_1$ and $E_2$ in Fig. 3(a). By using the two basic cell structures, the density product can be represented by contracting out the physical indices in the density matrix tensor in Fig. 3(b). As a consequence, the thermal fidelity can be presented in the tensor network representation in Fig. 3(b). The tFLS $d(\beta_1,\beta_2)$ is equivalent to the maximum eigenvalue of the transfer matrix [54].

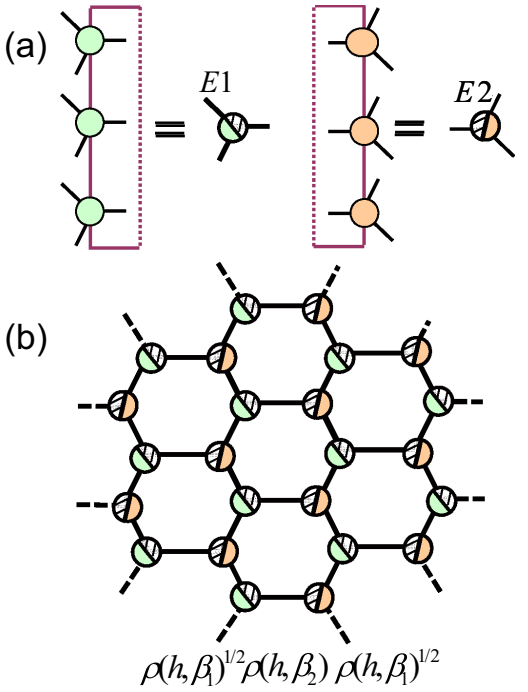


FIG. 3. (a) Two basic cell structures for $E_1$ and $E_2$. (b) Tensor network representation of the product $\rho(\beta_1)^{1/2}\rho(\beta_2)\rho(\beta_1)^{1/2}$.

Generally, in the tensor network representation of the thermal fidelity in Fig. 3(b), each bond dimension of the tensors $E_1$ and $E_2$ is $D^6$ and then a relatively-larger environment dimension $M$ is needed for reliable calculation results. Consequently, calculation of the thermal fidelity in the tensor network representation in Fig. 3(b) requires a lot of computational memory space and a long calculation time. In our case, however, all of the system parameters of the given Hamiltonian $H$ are fixed in calculating the thermal fidelity. This fact allows us to improve the computation efficiency because the thermal-state fidelity can be simplified due to $\rho = e^{-\beta H}$ as

$$F(\beta_1,\beta_2) = \frac{\mathrm{Tr}\,\rho(\tilde{\beta})}{\sqrt{\mathrm{Tr}\rho(\beta_1)}\sqrt{\mathrm{Tr}\rho(\beta_2)}}, \tag{14}$$

where $\tilde{\beta} = (\beta_1+\beta_2)/2$. With the effective temperature $\tilde{\beta} = (\beta_1+\beta_2)/2$, the simple form of the thermal fidelity in Eq. (14) is represented in the tensor network representation in Fig. 2(b). In the representation, each bond dimension of the maximum tensors $a$ and $b$ becomes $D^2$, where the tensors $a$ and $b$ correspond to the transfer matrices $E_1$ and $E_2$ in Fig. 3(b). This results in the representation dimensions of the tensors $a$ and $b$ being much smaller than those of the tensors $E_1$ and $E_2$. The consequential environment dimension $M$ becomes much smaller than that in Fig. 2(b). Thus, in our study, we have used the tensor network representation in Fig. 3(b) of the thermal fidelity in Eq. (14) with the effective temperature $\tilde{\beta} = (\beta_1+\beta_2)/2$. The computational cost of our algorithms scales like $D^3M^6$.

### A. Pinch points of tFLS

At zero temperature, the fidelity per lattice site (FLS) for quantum states has been applied successfully in the

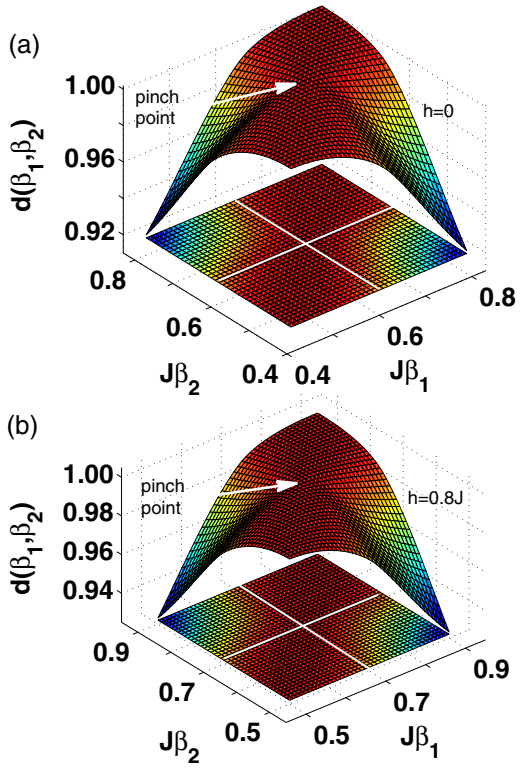


FIG. 4. Thermal fidelity per lattice site $d(\beta_1,\beta_2)$ for transverse magnetic fields (a) $h = 0$ and (b) $h = 0.8\,J$ in the $\beta_1 - \beta_2$ parameter space. Pinch points are indicated on the thermal fidelity surfaces. Also shown is the projection of the thermal fidelity surface onto the $\beta_1 - \beta_2$ plane, on which the intersection lines are indicated.

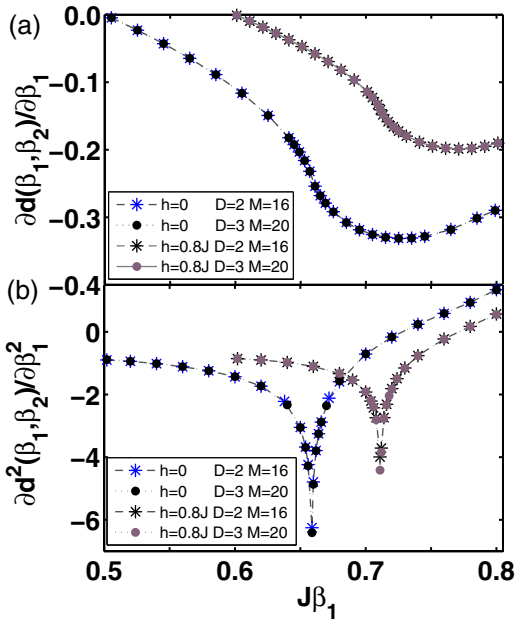


FIG. 5. (a) The first partial derivative of the thermal fidelity per site $\partial d(\beta_1,\beta_2)/\partial\beta_1$ as a function of $\beta_1$ for transverse magnetic fields $h = 0$ and $0.8\,J$ with $J\beta_2 = 0.5$ and 0.6, respectively. (b) The second partial derivative of the thermal fidelity per site $\partial d(\beta_1,\beta_2)/\partial\beta_1$ as a function of $\beta_1$. In (b), the singular points appear at $J\beta_c = 0.659$ and 0.711 for $h = 0$ and $0.8\,J$, respectively, which correspond to critical point estimates. For both (a) and (b), data are presented for different values of the bond dimension $D$ and environment truncation dimension $M$.

investigations of quantum phase transitions because it can capture unstable fixed points, corresponding to phase transition points, along renormalization group flows [18,54]. In a similar fashion, our tFLS can capture thermal phase transition points. Suppose that a thermal system undergoes thermal phase transitions at a critical temperature $T_c$ (or $\beta_c$), which may imply that the thermal state of the system experiences a nontrivial change of its structure. Such a nontrivial change in the thermal state can be captured by the tFLS. Specifically, $d(\beta_1,\beta_2)$ reveals singular behavior when $\beta_1$ ($\beta_2$) crosses $\beta_c$ for a fixed $\beta_2$ ($\beta_1$). At the point $(\beta_c,\beta_c)$, the singular behaviors can characterize a transition point, especially named as a pinch point $d(\beta_c,\beta_c)$ of the tFLS, which is the intersection of two singular lines $\beta_1 = \beta_c$ and $\beta_2 = \beta_c$ as a function of $\beta_1$ and $\beta_2$ for continuous phase transitions. Then there are two possible ways to investigate a thermal phase transition: (i) detecting pinch points on the tFLS surface and (ii) detecting singular behavior of the tFLS. For continuous phase transitions the second way is more practical. However, for discontinuous phase transitions the pinch points are obviously identified on the tFLS surface.

In Fig. 4, we plot the tFLS surface $d(\beta_1,\beta_2)$ for (a) $h = 0$ and (b) $h = 0.8\,J$ in the $\beta_1 - \beta_2$ parameter space for bond dimension $D = 2$ and the environment truncation dimension $M = 32$. The pinch points, obtained from the singularity behavior of the tFLS as discussed below, are identified. The accuracy of these results is discussed in Sec. V.

### B. Singular behavior of the tFLS

To determine phase transition points from the tFLS, we examine the singular behavior of the tFLS itself and its derivatives. We consider the tFLS $d(\beta_1,\beta_2)$ with a reference state $|\Psi(\beta_2)\rangle$ for a fixed value of $\beta_2$, i.e., $J\beta_2 = 0.5$ for $h = 0$ and $J\beta_2 = 0.6$ for $h = 0.8\,J$. In Fig. 5, we plot the (a) first- and (b) second-derivatives of tFLS $d(\beta,\infty)$ as a function of $\beta$ for $h = 0$ and $0.8\,J$. Here the value of the step is $Jd\beta = 10^{-3}$. The first derivatives are shown to be continuous, i.e., to exhibit nonsingular behavior. However, the second derivatives exhibit singular behavior showing a discontinuity. The discontinuous points indicate a thermal phase transition point. For bond dimension $D = 2$ and the environment truncation dimension $M = 32$ corresponding to Fig. 4, the critical temperatures are estimated as $k_BT_c/J = 1.51745$ ($J\beta_c = 0.659$) for $h = 0$ and $k_BT_c/J = 1.40647$ ($J\beta_c = 0.711$) for $h = 0.8\,J$. The convergence of these results with increasing values of $D$ and $M$ is apparent in Fig. 5 and discussed in Sec. V. The continuous behavior of both the fidelity surface in Fig. 4 and the first derivative in Fig. 5(a) imply that the system undergoes a continuous phase transition.

## IV. VON NEUMANN ENTROPY AT FINITE TEMPERATURE

In our tPEPS approach, we can use the thermal density matrix $\rho(h,\beta)$ in Fig. 2(b) to investigate whether finite-temperature phase transitions can be quantified by using

the von Neumann entropy. We consider two types of reduced density matrices, i.e., one-site reduced density matrix $\rho_{A/B}(h,\beta) = \mathrm{Tr}_{B/A\cup C}\ \rho(h,\beta)$ and two-site reduced density matrix $\rho_{A\cup B}(h,\beta) = \mathrm{Tr}_C\ \rho(h,\beta)$, where $C$ denotes the remainder of the system. The von Neumann entanglement entropy $S$ of a bipartition of the system is thus given in terms of the reduced density matrix

$$S_j = -\mathrm{Tr}\ \rho_j(h,\beta)\log_2 \rho_j(h,\beta), \tag{15}$$

where $\rho_j(h,\beta) = \mathrm{Tr}_{j^c}\ \rho(h,\beta)$, with $j = A, B$ or $A\cup B$, is the reduced density matrix obtained from the full density matrix by tracing out the degrees of freedom of the rest of the subsystem $j^c$.

In Fig. 6, we plot (a) the von Neumann entropies and (b) the derivatives as a function of the inverse temperature $\beta$ for the same values of the transverse magnetic fields $h = 0$ and $h = 0.8\,J$, with step value $Jd\beta = 10^{-4}$. In Fig. 6(a), the plots show that as temperature increases, both the one-site and the two-site von Neumann entropies increase due to the increment of thermal fluctuations and that they exhibit singular behavior. In Fig. 6(b), the derivatives of the von Neumann entropies show the singular points clearly. At the critical inverse temperatures $\beta_c$, the singular points correspond to the singular points of the tFLS for the same values of the bond dimension $D$ and environment truncation dimension $M$. It is thus shown that the one-site and the two-site von Neumann entropies capture the finite-temperature phase transitions in this model. Similar to the continuous behavior of quantum phase transitions [29,56], the continuous behavior of the von Neumann entropy at the singular points implies that a continuous phase transition occurs at the transition temperatures [57].

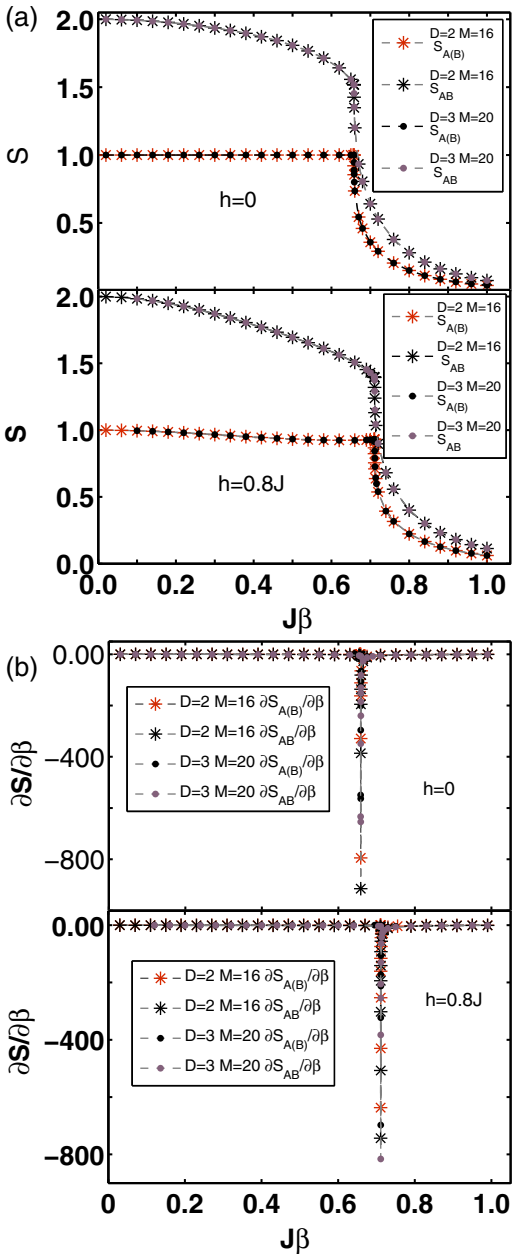


FIG. 6. (a) The von Neumann entropies $S$ and (b) the derivatives as a function of inverse temperature $\beta$ for transverse magnetic fields $h = 0$ and $0.8\,J$. The singular behavior of the von Neumann entropy is observed at $J\beta_c = 0.6585$ and 0.711 for transverse magnetic field $h = 0$ and $0.8\,J$, respectively. Data are presented for different values of the bond dimension $D$ and environment truncation dimension $M$.

## V. TRANSVERSE MAGNETIZATION

In order to confirm the results from the tFLS and the von Neumann entropy, we investigate the local order parameter, defined by the transverse magnetization, in this section. In the classical limit, i.e., $\beta = 0$, for the case of $h = 0$, the two site interaction gate $U_{zz}(\beta)$ acts on an initial state $|\Psi(0)\rangle$ and the exact state $|\Psi(\beta)\rangle = U_{zz}|\Psi(0)\rangle$ can be obtained. The bond dimension $D = 2$ is then enough for an exact iPEPS representation of any classical state including the critical one. However, the calculations of expectation values require an effective approximate environment. Thus, in the vicinity of the critical point, a bigger environment truncation dimension $M$ is required to calculate expectation values of operators such as magnetizations and spin correlations [46]. For the opposite limit, i.e., $\beta \to \infty$, which corresponds to the quantum case, the state of the system is in a product state configuration, where either every spin is in the $|\uparrow\rangle_z$ state or every spin is in the $|\downarrow\rangle_z$ state. Then the system exhibits a spontaneous symmetry breaking, which randomly chooses either the spin up or spin down configuration. According to Eqs. (10a) and (10b), the zero temperature ferromagnetic state $U_{zz}(\infty)|\Psi(0)\rangle$ is represented exactly by $\tilde{A}^{ia}_{s_l,s_u,s_r} \propto (-1)^{is}\delta^{ia}$ and $\tilde{B}^{ia}_{s_l,s_r,s_d} \propto (-1)^{is}\delta^{ia}$.

In Fig. 7, we plot the magnetization $M_Z = \langle\sigma_z\rangle$ as a function of the inverse temperature $\beta$ for transverse magnetic field at the values $h = 0$ and $0.8\,J$ with different values of the bond dimension $D$ and environment truncation dimension $M$ for the step value $Jd\beta = 10^{-4}$. The spontaneous magnetizations have nonzero value for the inverse temperatures $\beta > \beta_c$. Here $J\beta_c = 0.6585$ and 0.711 for transverse magnetic fields $h = 0$ and $0.8J$, respectively. These critical temperatures are the same as those obtained from the tFLS in Sec. III B and from the von Neuman entropy in Sec. IV.

With regard to the accuracy of our results, we show in Tables I and II estimates of the critical (inverse) temperature for transverse magnetic field values $h = 0$ and $0.8\,J$ with different values of the bond dimension $D$ and environmental truncation

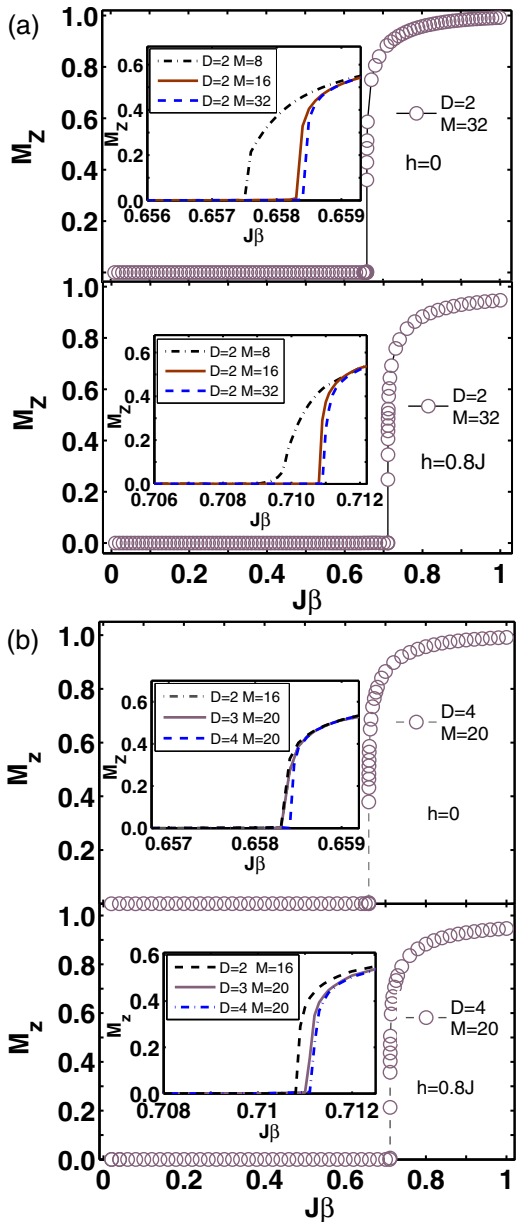


FIG. 7. Magnetization $M_z$ as a function of inverse temperature $\beta$ for transverse magnetic fields (a) $h = 0$ and (b) $0.8\,J$. The insets show the spontaneous magnetizations $M_Z$ plotted for different bond dimensions $D$ and environment truncation dimensions $M$. The critical inverse temperatures are estimated as $J\beta_c = 0.6585$ and 0.711 for transverse magnetic field $h = 0$ and $0.8\,J$, respectively.

TABLE I. Estimates of the inverse critical temperature $\beta_c$ for different bond dimensions $D$ and environment truncation dimensions $M$ for magnetic field $h = 0$.

| | $M = 8$ | $M = 10$ | $M = 16$ | $M = 20$ | $M = 32$ |
|---|---|---|---|---|---|
| $D = 2$ | 0.6576 | 0.658 | 0.6584 | 0.6584 | 0.6585 |
| $D = 3$ | 0.6576 | 0.6581 | 0.6584 | 0.6584 | |
| $D = 4$ | 0.6578 | 0.6581 | 0.6584 | 0.6585 | |

TABLE II. Estimates of the inverse critical temperature $\beta_c$ for different bond dimensions $D$ and environment truncation dimensions $M$ for magnetic field $h = 0.8\,J$.

| | $M = 8$ | $M = 10$ | $M = 16$ | $M = 20$ | $M = 32$ |
|---|---|---|---|---|---|
| $D = 2$ | 0.7099 | 0.7106 | 0.7109 | 0.7110 | 0.7110 |
| $D = 3$ | 0.7100 | 0.7108 | 0.7110 | 0.7111 | |
| $D = 4$ | 0.7102 | 0.7109 | 0.7110 | 0.7112 | |

dimension $M$. It is readily apparent that these estimates soon saturate to the number of significant figures shown.

## VI. PHASE DIAGRAM IN THE PRESENCE OF TRANSVERSE MAGNETIC FIELD

So far, we have studied the tFLS and the von Neumann entropy with characteristic singular behavior indicating finite-temperature phase transitions at the two magnetic field values cases $h = 0$ and $0.8\,J$ for the quantum transverse Ising model on the honeycomb lattice. In this section we investigate the phase boundary in the wider parameter space $0 \leqslant h/J \leqslant 1.9$. In determining the critical temperature and field, the accuracy of the iPEPS is more affected by the environment truncation dimension $M$ than the bond dimension $D$ (see Tables I and II). From our calculations, we have noticed that the practical optimized dimensions are the bond dimension $D = 2$ and the environment dimension $M = 16$ with the step value $Jd\beta = 10^{-3}$, which means that other choices for the dimensions would not change the numerical critical temperature within the errors of the accuracy of the iPEPS.

We have calculated twenty critical points including the case of zero-magnetic field for the model. In Table III, we summarize the critical temperatures $k_BT_c$ and the corresponding critical magnetic fields $h_c$ in units of the interaction strength $J$. In the temperature-magnetic field plane, we plot the phase boundary in Fig. 8. As the magnetic field increases, the critical temperature becomes lower. Note that Fig. 8 shows a monotonic behavior of the critical points in the temperature-magnetic field plane, which implies that the phase separation can be determined by a phase boundary function $f(T_c,h_c) = (k_BT_c/J)^2 + (h_c/J)^2/2$ with a single numerical fitting constant $a$, i.e., $f(T_c,h_c) = a$. Thus the model is in the ferromagnetic phase for $f(T_c,h_c) < a$, with a nonmagnetic phase for $f(T_c,h_c) > a$. A best numerical fitting is performed to give the fitting constant $a = 2.298(7)$. In Fig. 8, the dashed line is the fitted phase boundary. One can also estimate the critical temperature and field by using the fitted phase boundary $(k_BT_c)^2 + h_c^2/2 = aJ^2$. As the magnetic field varies, the critical temperature can be obtained by the relation $k_BT_c = \sqrt{aJ^2 - h^2/2}$. The critical temperatures can be estimated as, for instance, $k_BT_c/J = \sqrt{a} \simeq 1.516(2)$ for $h = 0$ and $k_BT_c/J \simeq 1.406(3)$ for $h = 0.8\,J$. Alternatively, as temperature varies, the critical field can be obtained by the relation $h_c = \sqrt{2aJ^2 - 2(k_BT)^2}$. The critical fields can be estimated as, for instance, $h_c/J = \sqrt{2a} \simeq 2.144(3)$ at $T = 0$ and $h_c/J \simeq 2.139(3)$ at $k_BT/J = 0.1$. In comparison with the numerical estimates, the fitted critical values shown in Table III have absolute errors less than around $10^{-3}$.

TABLE III. Critical temperature $k_BT_c(=1/\beta_c)$ for values of the magnetic field $h$ in the honeycomb spin lattice with quantum Ising interaction in units of the interaction strength $J$. The fitted critical temperature $k_BT_c^{\rm fit}$ was estimated by using the phase boundary function $(k_BT_c)^2+h^2/2=aJ^2$ with the numerical constant $a=2.298(7)$. The absolute error is defined as $\varepsilon_{\rm err}=|k_BT_c-k_BT_c^{\rm fit}|/(k_BT_c)$.

| $h$ | 0.0 | 0.1 | 0.2 | 0.3 | 0.4 | 0.5 | 0.6 | 0.7 | 0.8 | 0.9 |
|---|---|---|---|---|---|---|---|---|---|---|
| $\beta_c$ | 0.659 | 0.659 | 0.662 | 0.665 | 0.671 | 0.678 | 0.687 | 0.698 | 0.711 | 0.727 |
| $k_BT_c$ | 1.5175 | 1.5175 | 1.5106 | 1.5038 | 1.4903 | 1.4749 | 1.4556 | 1.4327 | 1.4065 | 1.3755 |
| $k_BT_c^{\rm fit}$ | 1.515(2) | 1.514(2) | 1.509(2) | 1.501(2) | 1.489(2) | 1.474(2) | 1.455(2) | 1.432(2) | 1.406(3) | 1.375(3) |
| $\varepsilon_{\rm err}$ | 0.002(1) | 0.002(2) | 0.0015(8) | 0.002(2) | 0.0016(7) | 0.0016(5) | 0.0016(2) | 0.00170(8) | 0.00177(6) | 0.0018(3) |
| $h$ | 1.0 | 1.1 | 1.2 | 1.3 | 1.4 | 1.5 | 1.6 | 1.7 | 1.8 | 1.9 |
| $\beta_c$ | 0.747 | 0.770 | 0.799 | 0.834 | 0.877 | 0.931 | 1.000 | 1.095 | 1.223 | 1.417 |
| $k_BT_c$ | 1.3387 | 1.2987 | 1.2516 | 1.199 | 1.1403 | 1.0741 | 1.000 | 0.9132 | 0.8177 | 0.7057 |
| $k_BT_c^{\rm fit}$ | 1.340(3) | 1.301(3) | 1.256(3) | 1.205(3) | 1.148(3) | 1.083(3) | 1.008(3) | 0.923(4) | 0.823(4) | 0.702(5) |
| $\varepsilon_{\rm err}$ | 0.002(2) | 0.002(2) | 0.004(2) | 0.005(2) | 0.007(3) | 0.008(3) | 0.009(3) | 0.011(4) | 0.007(5) | 0.007(5) |

Consequently, these results indicate that the phase boundary of the transverse Ising model on the honeycomb lattice with quantum Ising interactions is well described for finite $T$, where the thermal fluctuations are dominant, by the phase boundary function $(k_BT_c)^2+h_c^2/2=aJ^2$ with the single numerical fitting constant $a=2.298(7)$.

We note that if this simple curve was an exact result for *all* $T$, the constant value $a=4/[\ln(2+\sqrt{3})]^2=2.3063\ldots$ follows from (3). This value is close enough to the fitted value, but the inferred quantum critical point at $T=0$, $h_c/J=2\sqrt{2}/\ln(2+\sqrt{3})=2.1476\ldots$, where the quantum fluctuations dominate, leads to a discrepancy with the high precision Monte-Carlo estimate $h_c/J=2.13250(4)$ [48]. As is well known [2], the effect of quantum fluctuations remains significant in the vicinity of the quantum critical point ($T=0$), leading to interesting effects in the quantum critical region where the thermal and quantum fluctuations compete. In this study, we have concentrated on the effects of thermal fluctuations via the thermal fidelity and von Neumann entropy for finite temperature in the region where the fitted function applies. Understanding this discrepancy and the quantum critical region in general requires further refinement of the approaches used here.

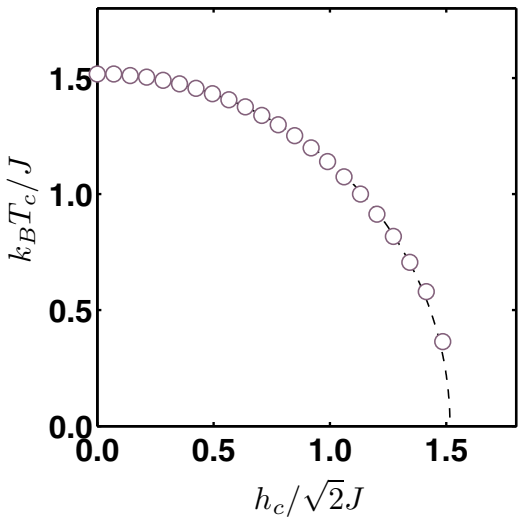


FIG. 8. Phase boundary in the temperature-magnetic field plane for the honeycomb lattice with quantum Ising interactions. The circles indicate the numerical data and the dashed line is the numerical fitting function $(k_BT_c)^2+h_c^2/2=aJ^2$ with $a=2.298(7)$.

## VII. CONCLUSION

We have investigated the phase boundary of the quantum transverse Ising model on the honeycomb lattice. To calculate the thermal ground state at finite temperature, we have employed the tPEPS algorithm with ancillas. In order to quantify the finite-temperature phase transition, we have used the von Neumann entropy and the thermal-sate fidelity defined as the overlap measurement between two thermal states. The tensor network representation of the tFLS has been constructed for thermal states on the honeycomb lattice. The tFLS and the von Neumann entropy have been shown to successfully detect the continuous phase transition points in the temperature-magnetic field plane.

The phase boundary in the temperature-magnetic field plane is found to be well-approximated by the curve $(k_BT_c)^2+h_c^2/2=aJ^2$ for finite $T$ with the single numerical fitting coefficient $a=2.298(7)$. Then for $(k_BT_c)^2+h_c^2/2<aJ^2$, the model is in the ferromagnetic phase and for $(k_BT_c)^2+h_c^2/2>aJ^2$ in the nonmagnetic phase. The fitted phase boundary estimates the critical temperature $k_BT_c/J=\sqrt{a}\simeq 1.516(2)$ at $h=0$, which agrees well with the exact result (3). On the other hand, at $T=0$ the fitted phase boundary estimates the quantum critical field $h_c/J=\sqrt{2a}\simeq 2.1443(3)$ compared to the known Monte Carlo estimate $h_c/J=2.13250(4)$ [48]. Understanding this discrepancy requires further refinement of the methods used here, which are applicable in the region where thermal fluctuations dominate. Similar quadratic curves for finite $T$ may possibly apply for the quantum transverse Ising model on other planar lattices. More importantly, our results show that the thermal fidelity and von Neumann entropy for finite temperature can be used to capture finite-temperature phase transitions. Thus the fidelity and the von Neumann entropy approaches can be extended to the corresponding thermal fidelity and von Neumann entropy approaches for finite temperature.

## ACKNOWLEDGMENTS

MTB gratefully acknowledges support from Chongqing University and the 1000 Talents Program of China. This work

is supported in part by the Fundamental Research Funds for the Central Universities (Projects No. 106112015CDJRC131215 and No. 106112016CDJXY300008) and the National Natural Science Foundation of China (Grants No. 11575037, No. 11374379, No. 11674042, and No. 11174375).

[1] L. D. Landau and E. M. Lifshitz, *Statistical Physics* (Pergamon, New York, 1958).
[2] S. Sachdev, *Quantum Phase Transitions* (Cambridge University Press, Cambridge, 2011).
[3] P. M. Chaikin and T. C. Lubensky, *Pinciples of Condensed Matter Physics* (Cambridge University Press, Cambridge, 1995).
[4] L. Amico, R. Fazio, A. Osterloh, and V. Vedral, Rev. Mod. Phys. **80**, 517 (2008).
[5] G. Vidal, J. I. Latorre, E. Rico, and A. Kitaev, Phys. Rev. Lett. **90**, 227902 (2003).
[6] P. Calabrese and J. Cardy, J. Stat. Mech.: Theory Exp. (2004) P06002.
[7] V. E. Korepin, Phys. Rev. Lett. **92**, 096402 (2004).
[8] L. Tagliacozzo, T. R. de Oliveira, S. Iblisdir, and J. I. Latorre, Phys. Rev. B **78**, 024410 (2008).
[9] F. Pollmann, S. Mukerjee, A. M. Turner, and J. E. Moore, Phys. Rev. Lett. **102**, 255701 (2009).
[10] Q.-Q. Shi, R. Orús, J. O. Fjærestad, and H.-Q. Zhou, New J. Phys. **12**, 025008 (2010).
[11] J.-M. Stéphan, G. Misguich, and F. Alet, Phys. Rev. B **82**, 180406(R) (2010).
[12] B.-Q. Hu, X.-J. Liu, J.-H. Liu, and H.-Q. Zhou, New J. Phys. **13**, 093041 (2011).
[13] J.-H. Liu, H.-T. Wang, Q.-Q. Shi, and H.-Q. Zhou, Phys. Lett. A **376**, 2677 (2012).
[14] I. Affleck and A. W. W. Ludwig, Phys. Rev. Lett. **67**, 161 (1991).
[15] X.-J. Liu, B.-Q. Hu, S. Y. Cho, H.-Q. Zhou, and Q.-Q. Shi, J. Korean Phys. Soc. **69**, 1212 (2016).
[16] S.-J. Gu, Int. J. Mod. Phys. B **24**, 4371 (2010).
[17] P. Zanardi and N. Paunković, Phys. Rev. E **74**, 031123 (2006).
[18] H.-Q. Zhou and J. P. Barjaktarevič, J. Phys. A: Math. Theor. **41**, 412001 (2008); H.-Q. Zhou, J.-H. Zhao, and B. Li, *ibid.* **41**, 492002 (2008).
[19] M. M. Rams and B. Damski, Phys. Rev. Lett. **106**, 055701 (2011).
[20] J.-H. Liu, Q.-Q. Shi, J.-H. Zhao, and H.-Q. Zhou, J. Phys. A: Math. Theor. **44**, 495302 (2011).
[21] S. Yang, S.-J. Gu, C.-P. Sun, and H.-Q. Lin, Phys. Rev. A **78**, 012304 (2008).
[22] S.-J. Gu, Chin. Phys. Lett. **26**, 026401 (2009).
[23] X.-M. Lu, Z. Sun, X. Wang, and P. Zanardi, Phys. Rev. A **78**, 032309 (2008); X. Wang, Z. Sun, and Z. D. Wang, *ibid.* **79**, 012105 (2009).
[24] S. Chen, L. Wang, S. J. Gu, and Y. Wang, Phys. Rev. E **76**, 061108 (2007).
[25] V. Mukherjee and A. Dutta, Phys. Rev. B **83**, 214302 (2011).
[26] L. Gong and P. Tong, Phys. Rev. B **78**, 115114 (2008).
[27] H.-L. Wang, J.-H. Zhao, B. Li, and H.-Q. Zhou, J. Stat. Mech. (2011) L10001.
[28] H. T. Wang, B. Li, and S. Y. Cho, Phys. Rev. B **87**, 054402 (2013).
[29] Y. H. Su, B.-Q. Hu, S.-H. Li, and S. Y. Cho, Phys. Rev. E **88**, 032110 (2013).
[30] Y.-W. Dai, S. Y. Cho, M. T. Batchelor, and H.-Q. Zhou, Phys. Rev. E **89**, 062142 (2014).
[31] P. Zanardi, P. Giorda, and M. Cozzini, Phys. Rev. Lett. **99**, 100603 (2007).
[32] H. T. Quan and F. M. Cucchietti, Phys. Rev. E **79**, 031101 (2009).
[33] N. Paunković and V. R. Vieira, Phys. Rev. E **77**, 011129 (2008).
[34] W.-L. You, Y.-W. Li, and S.-J. Gu, Phys. Rev. E **76**, 022101 (2007).
[35] J. Sirker, Phys. Rev. Lett. **105**, 117203 (2010).
[36] J. G. Brankov and N. S. Tonchev, Phys. Rev. E **85**, 031115 (2012).
[37] L. Wang, Y.-H. Liu, J. Imriška, P. N. Ma, and M. Troyer, Phys. Rev. X **5**, 031007 (2015).
[38] C. Li and Z. Song, Phys. Rev. A **92**, 062103 (2015).
[39] P. Schmoll and R. Orús, Phys. Rev. B **95**, 045112 (2017).
[40] J. Cao, X. Cui, Z. Qi, W. Lu, Q. Niu, and Y. Wang, Phys. Rev. B **75**, 172401 (2007).
[41] C. Castelnovo and C. Chamon, Phys. Rev. B **76**, 184442 (2007).
[42] V. Popkov and M. Salerno, Europhys. Lett. **84**, 30007 (2008).
[43] Y. Zhao, W. Li, B. Xi, Z. Zhang, X. Yan, S.-J. Ran, T. Liu, and G. Su, Phys. Rev. E **87**, 032151 (2013).
[44] W. J. Porter and J. E. Drut, Phys. Rev. B **94**, 165112 (2016).
[45] J. Jordan, R. Orús, G. Vidal, F. Verstraete, and J. I. Cirac, Phys. Rev. Lett. **101**, 250602 (2008); H. C. Jiang, Z. Y. Weng, and T. Xiang, *ibid.* **101**, 090603 (2008); R. Orús and G. Vidal, Phys. Rev. B **78**, 155117 (2008).
[46] P. Czarnik, L. Cincio, and J. Dziarmaga, Phys. Rev. B **86**, 245101 (2012); P. Czarnik and J. Dziarmaga, *ibid.* **90**, 035144 (2014); **92**, 035120 (2015).
[47] P. Czarnik and J. Dziarmaga, Phys. Rev. B **92**, 035152 (2015); P. Czarnik, J. Dziarmaga, and A. M. Oleś, *ibid.* **93**, 184410 (2016); P. Czarnik, M. M. Rams, and J. Dziarmaga, *ibid.* **94**, 235142 (2016).
[48] H. W. J. Blöte and Y. Deng, Phys. Rev. E **66**, 066110 (2002).
[49] R. J. Baxter, *Exactly Solved Models in Statistical Mechanics* (Academic Press, London, 1982), Chap. 6.
[50] R. M. F. Houtappel, Physica **16**, 425 (1950).
[51] G. Vidal, Phys. Rev. Lett. **98**, 070201 (2007).
[52] M. Suzuki, Phys. Lett. A **146**, 319 (1990).
[53] R. Orús and G. Vidal, Phys. Rev. B **80**, 094403 (2009).
[54] H.-Q. Zhou, R. Orús, and G. Vidal, Phys. Rev. Lett. **100**, 080601 (2008).
[55] M. A. Nielsen and I. L. Chuang, *Quantum Computation and Quantum Information* (Cambridge University Press, Cambridge, 2000).
[56] Y. H. Su, S. Y. Cho, B. Li, H. L. Wang, and H.-Q. Zhou, J. Phys. Soc. Jpn. **81**, 074003 (2012).
[57] S.-J. Gu, S.-S. Deng, Y.-Q. Li, and H.-Q. Lin, Phys. Rev. Lett. **93**, 086402 (2004).